Effect of feed body geometry on separation performance of hydrocyclone

Yang, Xinghua; Simmons, Mark J. H.; Liu, Peikun; Zhang, Yuekan; Jiang, Lanyue

DOI:
10.1080/01496395.2018.1548486

Effect of feed body geometry on separation performance of hydrocyclone

Xinghua Yang[1], Mark J. H. Simmons[2], Peikun Liu[1*], Yuekan Zhang[1], Lanyue Jiang[1]

1College of Mechanical and Electrical Engineering, Shandong University of Science and Technology, Qingdao, China 266590

2 School of Chemical Engineering, University of Birmingham, Birmingham, United Kingdom, B15 2TT

ABSTRACT

The occurrence~~misplacement~~ of coarse particles in overflow and fine particles in underflow are known problems in hydrocyclone separations. This paper proposes improved feed body design of a hydrocyclone and the effect of feed body geometry on the flow field and separation performance is investigated experimentally and theoretically using PIV and CFD respectively. The air core formation and the velocity field are in good agreement using both approaches. Further simulated results indicate that the tapered feed body causes a reduction in fines entrainment by underflow, suitable for fine particles classification. In contrast, the conical feed body is advantageous for eliminating short circuiting.

Key word：hydrocyclone, CFD, PIV , feed body, separation

1 Introduction

Hydrocyclones have been widely used for solid-liquid separations in minerals engineering, waste water treatment, petrochemical engineering and bioengineering due to their advantages of low investment and maintenance costs, low energy consumption and adjustable handling capacity[1-3]. A traditional hydrocyclone commonly consists of a cylindrical feed body with a central vortex finder, an inlet tube attached to the top of the cylinder and a conical section with a spigot at the bottom. When the slurry is injected from

the tangential inlet, the rotational fluid flow generates a centrifugal force, causing large and coarse particles to migrate towards the outer wall and aggregate in the underflow while small and fine particles migrate upwards to the overflow. However, the phenomenon of short-circuiting in the overflow is unavoidable in the traditional operation, resulting in entrainment of coarse particles by the overflow product. As reported in the literature[4], about 12～18 % of the feed is short-circuiting without being subjected to centrifugal force action. At the same time, the misplacement of fine particles in the underflow product is also inevitable in the separation process. Both affect the separation accuracy and efficiency of hydrocyclones to a great extent.

Recent studies[5-7] have shown that the geometric structure of vortex finder and the cylinder have a strong influence on the above phenomena. Some researchers have tried to change the thickness, insertion depth and the geometric structure of the vortex finder. Yang[8] reported that the size of the dispersed particles reduces with the reduction of the vortex finder diameter thereby improving the separation performance. Tang[9] simulated a Φ75 mm hydrocyclone and indicated that increasing the thickness of the vortex finder had little effect on fine particles separation and may even reduce the separation efficiency of coarse particles. Hwang[10] carried out a simulation of a Φ10 mm hydrocyclone and revealed that increasing the thickness of~~thickening~~ the vortex finder could increase the centrifugal effect but reduce the particle residence time, so its effect on improving the separation efficiency was quite limited.

The insertion depth of vortex finder greatly influences the separation performance of hydrocyclone. Some researchers agreed that its value should be set within a certain range of (0.28~0.93)D, where D denotes the diameter of the hydrocyclone. Martinez[11] inferred the optimum vortex finder length value corresponded to a vortex finder length-hydrocyclone total length ratio of 0.1. If the depth of the vortex finder tip was excessive, a substantial decrease

in efficiency may be observed due to the swirl generated at the bottom of the hydrocyclone. Ghodrat[12] showed that the effect of vortex finder length on the separation efficiency was much less significant than those of diameter and shape. They showed opposite trends at low and high feed solids concentrations due to different magnitudes and locations of large tangential velocities. Altering the vortex finder design may also minimize the coarse particle misplacement in the overflow. A mantle-shaped vortex finder[13] was shown to reduce the pressure drop by 10 % and increase the separation efficiency by 5 %-10 % for fine particles. Hwang[10] also proposed that installing conical structures on the outer surface of the vortex finder was beneficial for improving the particle separation efficiency and reducing the cut-size. In general, the space between the vortex finder and the cylinder changed after using above mentioned structures, resulting in the improvement of the separation performance. Furthermore, some researchers have begun to study the direct optimization of cylinder structure. Delgadillo[14] explored alternative geometries of the cylinder using Computational Fluid Dynamics (CFD) modelling and observed great improvement during the classification of coarse particles, although there was a small increase in the by-pass of the very fine sizes. Also, some studies[15-17] paid attention to the influence on classification induced by inlet configuration and diameter.

Many researches focused on hydrocyclones with different conical configurations. Ghodrat [18] found that the cyclone performance was sensitive to both the length and shape of the conical section, and proposed an improved cyclone design by introducing a long convex cone ~~design~~. Minkov[19,20] considered the interaction of particles in a polydisperse suspension and investigated the direct modelling of the Fish-Hook effect in hydrocyclone separation, which could give an explanation of the non-monotonic character of the separation curve. Vakamalla [21] proposed several different conical designs and found that the cut size was 16_μm for conventional design, whereas the modified designs showed

values in the range of 8–13 μm.

CFD is a useful and reliable method for exploring novel design and simulating the operating performance of hydrocyclone[22-24]. The extensive studies of numerical simulation on hydrocyclone include, for example, the flow field characteristic, the comparison between different simulation models, the formation or elimination of air-core and its influence on the flow field. Wang[25] pointed out that the combined RSM turbulent model, stochastic Lagrangian model and VOF model can satisfactorily describe the flow and performance of a standard hydrocyclone, including the formation of the~~an~~ air core. Kuang [26] adopted the mixture multiphase model and RSM model to simulate the gas–liquid–solid flow in classifying hydrocyclones and investigated the effects of feed solids concentration on the separation performance. Ghodrat[27] used Eulerian–Eulerian model to study the multiphase flows to overcome the inaccuracy of the mixture model in describing the behaviors of different sized particles with a wide density range. Sripriya[28] simulated the flow field inside the hydrocyclone during separation process for both with and without air core. It was concluded the flow field characteristics inside the hydrocyclone with insertion of central solid rod became more suitable for separation. Similar studies by Evans[29] revealed that the separation performance could only be improved with the proper size of the inserted-rod. The pressure loss in the hydrocyclone was also found to be reduced when replacing the air core by inserting a rod. Further studies by Zou[30] stressed the relationship between flow rate and air core diameter. It was found that the flow condition had a non-monotonic effect on the diameter of the air core. In addition, more and more studies have laid emphasis on the verification of the simulation accuracy by different experimental methods including Laser Doppler Anemometry(LDA) and Particle Image Velocimetry (PIV). Marins[31] studied the three-dimensional flow characteristic in a hydrocyclone aimed at applications in the petroleum industry through the LDA and PIV techniques. Cui[32]carried out numerical

studies on the basis of CFD simulation and PIV measurements and showed that the axial and tangential velocities increased with the feed rate, and the enlargement of cone angle and overflow outlet diameter could speed up the overflow discharge rate.

This paper aims to explore hydrocyclones with newly designed feed body geometry using CFD and PIV respectively, for improving the separation efficiency with a reduction in the coarse and fine particles misplacement. In this study, a Φ40 mm hydrocyclone with conical or tapered feed body has been designed and the comparison between the traditional cylindrical feed body and the new designs is shown in Fig. 1. For convenience of analysis, the cone angle of the new feed body is defined as Φ, which is 10° and 25° for the conical feed body and tapered body respectively. ~~And in l~~Later in this study of cone angle effect on the flow field, Φ is changed to 8°, 9°, 12° ,15° for conical feed body and 15°，20°，30°, 35° for tapered feed body. It should be noticed that although the feed body configuration is changed, the total volume of the feed body is left unchanged compared with the traditional cylindrical design, aiming to keep the same capacity for the hydrocyclones with different feed body. Compared with the traditional structure, the cross-section area near the feed inlet in the new designs is changed. The changing area is expected to accelerate the velocity of the internal fluid, leading the solid particles to migrate quickly from the overflow conduit thus reducing the amount of short-circuiting. In order to justify the correctness of simulated method, the air-core formation and velocity distribution in the hydrocyclone with conical feed body are firstly simulated using multiphase flow Volume of fraction (VOF) model and turbulent Reynolds stress model (RSM), and then compared with PIV experimental data. The flow field and particle separation performance of the traditional hydrocyclone and new designs are analyzed computationally using RSM and Discrete phase model (DPM). The effectiveness of changing the feed body geometry on the particle separation efficiency is examined.

Fig. 1 Geometrical structure of hydrocyclone with different feed body

2 Methodology

2.1 CFD simulation

The CFD simulations were carried out using ANSYS Fluent 14.5. The geometry of the hydrocyclones and 3D meshes were created using ANSYS ICEM meshing tool. The unstructured hexahedral meshes were employed and the mesh sizes were approximately 65000 for each design, as shown in Fig. 2.

Fig. 2 Mesh of hydrocyclone with different feed body

The fluid flow was simulated using a segregated, transient-state, 3D implicit numerical solver supplied by Fluent. Flow governing equations in terms of Navier-Stokes equations were coupled using the SIMPLE algorithm and solved. The turbulence inside the hydrocyclone was simulated on the basis of RSM. PRESTO and Quick scheme were used to calculate pressure interpolation and solve dispersed phase transport equations respectively. The multi-phase flow was simulated using VOF and DPM. The dispersion medium was water with a density of 1000 kg m^{-3} and a viscosity of 1.0×10^{-3} Pa s. Silica particles with a density of 2650 kg m^{-3} were used as a particulate sample. The volume concentration of suspension was set as 3 %. The size distribution was that, 1 μm (18 %); 10 μm (26 %); 20 μm (28 %); 30 μm (18 %); 40 μm (8 %); 50 μm (2 %). The boundary conditions included no-slip on solid walls, a uniform velocity inlet and two constant pressure outlets of atmosphere. The convergence criteria were set as below 10^{-5} for the residuals of continuity and velocity.

2.1.1 RSM model

Turbulence is modelled using RSM, which is suitable for an isotropic turbulence such as in a hydrocyclone flow. Transport equations of Reynolds stresses terms are written as follows:

$$\frac{\partial}{\partial t}\left(\rho\overline{u_i'u_j'}\right)+\frac{\partial}{\partial x_k}\left(u_k\rho\overline{u_i'u_j'}\right)=P_{ij}+D_{T,ij}+D_{L,ij}+\varepsilon_{ij}+\emptyset_{ij}+F_{ij} \quad (1)$$

Here P_{ij} is stress production, $D_{T,ij}$ is turbulent diffusion, $D_{L,ij}$ is molecular diffusion , ε_{ij} is

dissipation ,φ_{ij} is pressure strain , F_{ij} is production by system rotation.

$$P_{ij}=-\rho\left(\overline{u_i'u_k'}\frac{\partial u_j}{\partial x_k}+\overline{u_j'u_k'}\frac{\partial u_i}{\partial x_k}\right) \tag{2}$$

$$D_{T,ij}=\frac{\partial}{\partial x_k}\left(\frac{\mu_t}{\sigma_k}\frac{\partial\overline{u_i'u_j'}}{\partial x_k}\right) \tag{3}$$

$$D_{L,ij}=\frac{\partial}{\partial x_k}\left(\mu\frac{\partial\overline{u_i'u_j'}}{\partial x_k}\right) \tag{4}$$

$$\varepsilon_{ij}=-2\mu\overline{\frac{\partial u_i'}{\partial x_k}\frac{\partial u_j'}{\partial x_k}} \tag{5}$$

$$\emptyset_{ij}=\overline{p'\left(\frac{\partial u_i'}{\partial x_j}+\frac{\partial u_j'}{\partial x_i}\right)} \tag{6}$$

$$F_{ij}=-2\rho\Omega_k\left(\overline{u_j'u_m'}e_{ikm}+\overline{u_i'u_m'}e_{jkm}\right) \tag{7}$$

The model requires the following empirical constants: $C_{1\varepsilon}=1.44$, $C_{2\varepsilon}=1.92$, $C_{\mu}=0.09$, $\sigma_k=0.82$, $\sigma_{\varepsilon}=1.0$.

2.1.2 VOF model

To model the interface between water and air in a hydrocyclone, the VOF free multiphase flow model is used. The tracking of the interface between the phases is accomplished by solving the continuity equation (8) and momentum equation (9).

$$\frac{\partial(\alpha_q)}{\partial t}+u_j\frac{\partial(\alpha_q)}{\partial x_i}=0 \tag{8}$$

$$\frac{\partial}{\partial t}(\rho u_j)+\frac{\partial}{\partial x_j}(\rho u_i u_j)=-\frac{\partial p}{\partial x_j}+\rho g_j+\frac{\partial}{\partial x_j}\mu\left(\frac{\partial u_i}{\partial x_j}+\frac{\partial u_j}{\partial x_i}\right) \tag{9}$$

Here α_q is volume fraction of q_{th} phase in the computational cell.

2.1.3 DPM model

The motion of a particle is described by the Stochastic Lagrangian multiphase flow model. Assume the volume fraction of dispersed phase is very low, and the particle-particle interactions and their effect on the liquid phase are negligible. The particle motion equation can be written as follows:

$$\frac{du_p}{dt} = F_D\left(\vec{u} - \overrightarrow{u_p}\right) + \frac{\vec{g}(\rho_p - \rho)}{\rho_p} \quad (10)$$

$$F_D = \frac{18\mu}{\rho_p d_p^2}\frac{C_D Re_p}{24} \quad (11)$$

$$Re_p = \frac{\rho d_p \left|\overrightarrow{u_p} - \vec{u}\right|}{\mu} \quad (12)$$

Here $F_D\left(\vec{u} - \overrightarrow{u_p}\right)$ is the drag force acting on the particle, where $\vec{u}$ and $\overrightarrow{u_p}$ are continuous phase velocity and particle velocity respectively, ρ_p and ρ are particle density and fluid density respectively, C_D is drag coefficient, which is determined by well-known drag models proposed by Wen[33] and Ergun[34]. Re_p is particulate Reynolds number, μ is fluid viscosity, d_p is particle diameter.

2.2 PIV test

In order to investigate the air-core formation process and flow field characteristic in the new type of hydrocyclone, the PIV test apparatus was set up as shown in Fig. 3. The circulation system was comprised of a water tank, a centrifugal pump, pipelines and Φ40 mm hydrocyclone with conical feed body. The hydrocyclone used in the experiment was made of transparent polymethylmethacrylate. The water volumetric flow rate was measured by a rotary flow meter (LWGY-20) and the inlet flow rate was controlled to 2 $m^3\ h^{-1}$. During the experiment, the pure water in the water tank was firstly pumped into the hydrocyclone, and then after the flow field became stable, polystyrene powder (10 μm, 1050 $kg\ m^{-3}$) was added as tracer particle. The motion trajectory of the tracer particles was captured and recorded. The 2-D PIV measurements were performed using PIV system (Dantec Dynamics, Denmark) . The system comprises dual cavity flash-pumped Nd:YAG lasers designed for PIV applications , synchronized to a single FlowSense EO 4M CCD camera (2048×2048 $pixels^2$) using a synchronizer attached to a personal computer. The PIV system was controlled using Dynamic Studio software. PIV measurement was carried out to obtain detail flow velocities over a vertical plane passing the central axis of the hydrocyclone. The air core formation was

captured using the CCD camera directly. In this test, the time interval Δt between twice exposure is 53300 μs . Totally 50 images are recorded for air-core formation under the flow rate condition of 2 m^3 h^{-1}.

Fig. 3 Schematic of PIV test apparatus: (a) test rig (1-hydrocyclone with conical feed body; 2-transparent box; 3-water tank; 4-pump; 5-flowmeter; 6-pressure gauge) ; (b) PIV measurement system; (c) photo of hydrocyclone

3 Results and discussion

The air-core formation and velocity distribution in the hydrocyclone with conical feed body, including the axial velocity and radial velocity, are firstly compared by using PIV test and CFD simulation respectively. Then, the comparisons of flow field characteristics in the hydrocyclone with different feed body structure are provided. The pressure distribution, velocity distribution and separation performance are investigated in detail by using the CFD simulation. Finally, the effects of cone angle on the flow field of hydrocyclones with conical and tapered feed body are presented.

3.1 Air-core and fluid velocity comparison

The air-core is an important flow characteristic in the hydrocyclone and it plays a great role in the separation performance. Fig. 4 shows the air-core formation process obtained from both the CFD simulations and PIV experiments. The fluid enters the hydrocyclone from the tangential inlet and rotates rapidly downwards along the wall. The air is squeezed and excluded in the middle area. At the beginning, the interface between the air and surrounding water is not stable. Then, a low pressure area at the intermediate area is gradually formed after the liquid fills the hydrocyclone and becomes stable. Due to the existence of low pressure area, the air is sucked from both the overflow conduit and underflow conduit. As a result, it forms a steady air-core. From the simulation result, the air-core formation time is 0.78 s. In the experiment, the liquid enters from inlet at 0.589 s and

the stable air-core is obtained at 1.360 s, therefore the formation time is 0.771 s, showing good agreement with the numerical simulation at the same condition.

Fig. 4 Air-core formation

The shape of the air-core is affected by position inside the hydrocyclone. An apparent twisting spiral state of the air-core near the apex can be observed from both the simulation and experiments. The reason may be that the cone section of hydrocyclone is the main separation area, so the multiphase flow, i.e., liquid, solid particles and air migrate in different directions and form complex turbulent structures. Especially in the bottom area, the narrow space causes a violent and chaotic flow, prompting the twisting air-core in this region. Also, an irregular expanding of air-core can be found inside the overflow conduit, as shown in the last two pictures of Fig. 4. It can be attributed to the combined effect of close distance to the overflow conduit wall and rapid inner vortex flow. In contrast, the air-core in the middle part of the hydrocyclone seems steady compared with that near the vortex finder and apex. Nevertheless, its diameter appears smaller, which is in agreement with previous studies [35]. With more separation space provided in the middle part, the flow field becomes stable. The rising pressure suppresses the growth of air-core, thus it shrinks.

Fig. 5(a) presents the velocity vector distribution in the conical feed body from PIV. In order to prevent the CCD camera from damage caused by strong reflection to Laser due to the existence of air-core, only less than half of the flow field is captured. This will not affect the whole velocity field analysis considering the symmetric characteristic of velocity distribution. It can be seen that the velocity vectors represent the typical flow characteristic in a hydrocyclone, that is, the outer free vortex and inner forced vortex, where the flows are directed downward near the hydrocyclone wall and upward near the central axis respectively. Fig. 5(b) and 5(c) present the PIV velocity components and corresponding CFD values for a horizontal transect taken at a height y = 123.6 mm, shown in Fig 5(a). This position

corresponds to the cross section near the bottom of vortex finder. Axial and radial velocity components agree within 12 %, which acts to validate the simulation. Therefore, the numerical simulation can be used to investigate the flow field and compares the effect of different structure on separation performance of the hydrocyclone.

Fig. 5 Velocity distribution at the bottom of vortex finder

3.2 Flow field

3.2.1 Pressure distribution

Fig. 6 plots the predicted pressure distributions along a horizontal plane crossing the central axis in the conventional and new types of hydrocyclone. For convenience of analysis, three representative heights are selected, z = 180 mm (representing cone section), z = 220 mm (representing feed body) and z = 248 mm / 281 mm / 227 mm (representing the cross section with a distance of 5 mm to the bottom of vortex finder), as shown in Fig. 1. The static pressure appears a symmetric distribution. For all types of hydrocyclone, the pressure reaches its maximum near the wall, and then decreases from the wall to the central axis. At the area near the centre, it reduces sharply and forms a negative pressure region, which will be occupied by the air from both the overflow and underflow conduit as it forms. Certain pressure drop from the wall to the centre can be observed, which influences the energy consumption and handling capacity to some extent.

Fig. 6 Pressure distribution at different section

Particles with different sizes or densities also have different response to the pressure gradient along the radial direction, explaining the particle separation mechanism. Comparison of the pressure gradient in the radial direction for each different section reveals that it is lowest in the conical body and largest in the tapered body. Usually, the pressure drop has direct impact on the tangential velocity. The higher pressure drops, the superior tangential velocity components can be obtained. The reason can be attributed to an ascending

centrifugal force, leading to an improved separation performance for particles.

3.2.2 Tangential velocity

The tangential velocity is the main factor that affects the solid-liquid separation. Fig. 7 shows the representative tangential velocity distribution at different cross section in the hydrocyclone. All of the tangential velocity distribution curves show good symmetry and the same shape, with an "M" curve can be observed along the radius. From the central axis to the wall, the tangential velocity firstly increases sharply, then as it reaches the peak point it begins to decrease, finally becomes to zero at the inner wall. The radial position where the maximum tangential velocity appears is nearly the same. The velocity comparison indicates that, at the same cross section, the tangential velocity in the tapered body is highest, in correspondence to the former pressure drop. High tangential velocities benefit the separation efficiency of coarse particles. Therefore, it is expected that the tapered type has a smaller cut-size while the conical type has a coarser cut-size.

Fig. 7 Tangential velocity distribution at different section

3.2.3 Axial velocity and Locus of zero vertical velocity (LZVV)

The axial velocity affects the residence time of particles to a great extent. Fig. 8 compares the axial velocity at different cross section heights for each design. The axial velocity distributes symmetrically. It is negative near the side wall and becomes positive along the radial direction to the central axis. Inside the hydrocyclone, all the points representing zero axial velocity connect together and form a LZVV. The LZVV is an interface. The fluid inside it flows upward and forms inner spiral flow. On the contrary, the fluid outside it flows downward and forms outer spiral flow. It is obvious the ascending amplitude of the velocity is high in the inner spiral flow, beneficial for fine particles migrate upward rapidly. For the tapered body, the axial velocity in the inner spiral shows more ascending gradient than that in other two types (see Fig. 8.(a) and (b)), reflecting a possible

reduction of fine particles entrainment by underflow and thereby increases its separation efficiency. While for the conical body, the axial velocity near the central axis appears higher than that in the cylindrical and tapered type at the cross section near the bottom of overflow tube (see Fig. 8(c)) It is advantageous for accelerating the particles' motion, making them move far away the overflow tube quickly and avoid the direct discharge with the upward liquid, that is, the short-circuiting.

Fig. 8 Axial velocity distribution at different section

The effect can also be verified in the LZVV diagram, as shown in Fig. 9. The LZVV diagram distorts obviously in the upper part of the conventional hydrocyclone. At the same cross section, the axial velocity becomes zero for many times along the radial direction, attributing to the combined influence of circulation flow and short-circuiting flow. Considering the velocity distribution curve simultaneously, it can be found the velocity value nearby is low. As a result, some solid particles are hard to move downward and may migrate into the overflow conduit directly, leading the local region an inefficient separation zone and reducing the separation efficiency. However, the defect can be overcome in the improved design, especially for the conical feed body. As shown in Fig. 9 (b), the LZVV line is clear and the zero trajectories reduce significantly near the overflow conduit. The increase of axial velocity can make the fluid flow move downward after it is introduced from the inlet, and then participate in the separation process. Therefore, the short-circuiting flow can be reduced and the misplacement of coarse particles in the overflow can be improved effectively. In a tapered type, there is little improvement of the phenomenon near the overflow conduit.

Fig. 9 LZVV diagram

3.2.4 Separation performance

The separation performance of the hydrocyclone is highly size dependent, and hence

particles with different sizes are separated with different efficiency. The grade efficiency curve can reflect the mass percentage of characteristic particle size entering the underflow, which is an important evaluation index of the hydrocyclone. Besides, the cut-size d_{50} can also be obtained from the grade efficiency curve. Usually, particles near cut-size have an equal chance to pass through overflow or underflow during the separation process.

As shown in Fig. 10, the grade efficiency curves of three types of hydrocyclone are plotted from the simulated data. It can be inferred that, the cut-size d_{50} of the tapered, cylindrical and conical type hydrocyclone are 11.25 μm, 13.05 μm and 17.95 μm respectively. Obviously, the smallest cut-size can be obtained by using the tapered type. The recovery rate of fines (such as 1 μm particles), is 22.17 %, 23.56 % and 29.29 % respectively, showing an effective reduction of fine particles in the underflow product by using the tapered hydrocyclone. Therefore, it is suitable for fine particles classification. While for the conical type, the enhanced cut-size indicates it is more favorable for particle sorting separation.

Fig. 10 Grade efficiency curve

3.3 Effect of cone angle

3.3.1 Conical feed body

The likely influence of different feed body cone angle on the flow field and separation performance can also be investigated using the numerical simulation. Fig. 11(a)(b)(c) show the distribution of static pressure, axial and tangential velocity over a diameter line at the height z = 220 mm. It can be seen that with ascending cone angle, the pressure distribution trend is consistent and the pressure drop increases gradually along the radial direction. As mentioned above, it is advantageous for increasing the tangential velocity thereby intensifying the separation process. When the cone angle exceeds 10°, there is little difference between the velocity values. The similar variation trend can be found for the tangential velocity at the same position. With the increase of cone angle, not only the

tangential velocity increases, but also the region of forced vortex and free vortex changes. From Fig. 11 (b), the radial position corresponding to the maximum tangential velocity value moves towards the central axis. In other words, the region of free vortex enlarges whilst that of the forced vortex shrinks. It should be also observed that tangential distribution has little difference when the conical angle is 10°, 12° and 15°. From Fig. 11 (c), the cone angle also has certain influence on the axial velocity, especially for the inner spiral flow, where velocity increases. This is beneficial for avoiding coarse particles misplacement in the overflow product. Fig. 11(d) gives the effect of feed body cone angle on grade efficiency curve. There is slight difference for fine particles separation when the cone angle changes. It can be inferred that the conical body hydrocyclone has a minimum cut-size of 17.95 μm when the cone angle is 10°. Simultaneously, the recovery rate of coarse particles in the underflow is highest, showing an improving effect on short circuiting and separation efficiency at given conditions.

Fig.11 Effect of Cone angle on flow field and separation performance in conical feed body

3.3.2 Tapered feed body

In order to study the influence of cone angle on the separation performance in hydrocyclone with tapered feed body, a series of feed body cone angle, 15°, 20°, 25°, 30°and 35° are simulated. The variation of static pressure, tangential velocity, axial velocity, and grade efficiency curve are plotted in Fig. 12. From Fig. 12(a)(b)(c), the pressure gradient along the radial direction shows an ascending tendency with the increase of cone angle, indicating an increasing centrifugal force. The trend of tangential velocity appears similar therefore an improved separation efficiency would be expected. The axial velocity comparison shows obvious enhancement in the inner spiral flow while little variation in the outer spiral flow. However, from Fig. 12(d), the cut-size increases slightly as the cone angle increases from 15° to 35°, proving that the cone angle has limited effect on the separation

performance of hydrocyclones with the tapered feed body.

Fig.12 Effect of Cone angle on flow field and separation performance in tapered feed body

4 Conclusions

The traditional cylinder of the hydrocyclone is changed to conical and tapered structure in order to reduce coarse particles misplacement in overflow and fine particles in underflow. The flow field and separation performance are investigated experimentally and theoretically using PIV and CFD. The main conclusions include:

(1) PIV test results of axial velocity and radial velocity are in good agreement with the numerical simulation results. The air-core formation conforms to the simulation results, verifying the accuracy of the numerical simulation method.

(2) The diameter of air-core is not uniform along the central axis, with a steady form in the middle part while an irregular shape inside the vortex finder and twisting appearance at the apex.

(3) For the feed with same particles size distribution, the cut-size of the tapered, cylindrical and conical type hydrocyclone is 11.25 μm, 13.05 μm and 17.95 μm respectively. The tapered feed body can effectively reduce fines entrainment in underflow, increase the separation efficiency and is suitable for fine particles classification. In contrast, the conical feed body is advantageous for eliminating short circuiting, increasing the cut-size and is suitable for particle sorting application.

(4) The cone angle of feed body has certain effect on internal flow field for hydrocyclones with conical and tapered structure. Both the static pressure and velocity increase gradually as the cone angle increases.

Acknowledgement

The work is funded by the National Natural Science Foundation of China (21276145) and

Natural Science Foundation of Shandong Province（ZR2016EEM37）.

References

1 Schuetz, S.; Mayer, G.; Bierdel, M., et al. (2004) Investigations on the flow and separation behaviour of hydrocyclones using computational fluid dynamics. *Int. J. Miner. Process*, 73:229-237.

2 Otto, N.; Platz, S.; Fink, T. ,et al.. (2016) Removal of micropollutants with coarse-ground activated carbon for enhanced separation with hydrocyclone classifiers. *Water Sci. Technol.* 73:2739-2746.

3 Bicalho, I. C.; Mognon, J. L.; Shimoyama, J., et al. (2013) Effects of operating variables on the yeast separation process in a hydrocyclone, *Sep. Sci. Technol*. 48:915-922.

4 Xu, J. R.; Luo, Q.; Qiu, J. C.. (1991) Research on the preseparation space in hydrocyclones. *Int. J. Miner. Process.* 31 1-10.

5 Chu, L. Y.; Chen, W. M.; Lee, X. Z.. (2000) Effect of structural modification on hydrocyclone performance. *Sep. Purif. Technol.* 21:71-86.

6 Vieira, L. G. M.; Damasceno, J. J.; Barrozo, M. A.. (2010) Improvement of hydrocyclone separation performance by incorporating a conical filtering wall. *Chem. Eng. Process*. 49:460-467.

7 Vieira, L. G. M.; Silvério, B. C.; Damasceno, J. J.,et al. (2011) Performance of hydrocyclones with different geometries. *Can. J. Chem. Eng.* 89:655-662.

8 Yang, Q.; Wang, H.; Wang, J., et al. (2011) The coordinated relationship between vortex finder parameters and performance of hydrocyclones for separating light dispersed phase. *Sep. Purif. Technol.* 79:310-320.

9 Tang, B.; Xu, Y.; Song, X., et al. (2015) Numerical study on the relationship between high sharpness and configurations of the vortex finder of a hydrocyclone by central composite

design. *Chem. Eng. J.* 278:504-516.

10 Hwang, K. J.; Chou, S. P.. (2017) Designing vortex finder structure for improving the particle separation efficiency of a hydrocyclone, *Sep. Purif. Technol.* 172:76-84.

11 Martínez, L. F.; Lavín, A. G.; Mahamud, M. M., et al. (2008) Vortex finder optimum length in hydrocyclone separation. *Chem. Eng. Process*. 47:192-199.

12 Ghodrat, M.; Kuang, S. B.; Yu, A. B.,et al. (2014) Numerical analysis of hydrocyclones with different vortex finder configurations. *Miner. Eng.* 63:125-138.

13 Wang, B.; Yu, A. B.. (2008) Numerical study of the gas–liquid–solid flow in hydrocyclones with different configuration of vortex finder. *Chem. Eng. J.* 135:33-42.

14 Delgadillo, J. A.; Rajamani, R. K.. (2007) Exploration of hydrocyclone designs using computational fluid dynamics. *Int. J. Miner. Process.* 84:252-261.

15 Vieira, L. G. M.; Silva, D. O.; Barrozo, M. A. S.. (2016) Effect of inlet diameter on the performance of a filtering hydrocyclone separator. *Chem. Eng. Technol.* 39:1406-1412.

16 Zhang, C.; Wei, D.; Cui, B.,et al. (2017) Effects of curvature radius on separation behaviors of the hydrocyclone with a tangent-circle inlet. *Powder Technol.* 305:156-165.

17 Zhang, C.; Cui, B.; Wei, D.,et al. (2017) Predicting the optimum range of feed flow rate in a hydrocyclone using the method combined flow pattern and equation model. *Powder Technol.* 319:279-288.

18 Ghodrat, M.; Kuang, S. B.; Yu, A. B., et al. (2014). Numerical analysis of hydrocyclones with different conical section designs. *Miner. Eng.* 62:74-84.

19 MinKov, L. L.; Dueck, J. H. (2012) Numerical modeling of a nonmonotonic separation hydrocyclone curve. *J. Eng. Phys. Thermophys*. 85(6):1317-1326.

20 MinKov, L. L.; Dueck, J. H.; Neesse, T. (2014). Computer simulations of the Fish-Hook effect in hydrocyclone separation. *Miner. Eng.* 62:19-24.

21 Vakamalla, T. R.; Koruprolu, V. B. R.; Arugonda, R.,et al. (2017) Development of novel

hydrocyclone designs for improved fines classification using multiphase CFD model. *Sep. Purif. Technol.* 175:481-497.

22 Delgadillo, J. A.; Rosales, M. G.; Perez, A. C.,et al. (2013) CFD analysis to study the effect of design variables on the particle cut size in hydrocyclones. *Asia-Pac. J. Chem. Eng*. 8:627-635.

23 Mokni, I.; Dhaouadi, H.; Bournot, P., et al. (2015) Numerical investigation of the effect of the cylindrical height on separation performances of uniflow hydrocyclone. *Chem. Eng. Sci.* 122:500-513.

24 Vakamalla, T. R.; Mangadoddy, N. (2017). Numerical simulation of industrial hydrocyclones performance: Role of turbulence modelling. *Sep. Purif. Technol.* 176:23-39.

25 Wang, B.; Chu, K. W.; Yu, A. B. (2007). Numerical Study of Particle− Fluid Flow in a Hydrocyclone. *Ind. Eng. Chem. Res.* 46(13):4695-4705.

26 Kuang, S. B.; Chu, K. W.; Yu, A. B. , et al. (2012). Numerical study of liquid–gas–solid flow in classifying hydrocyclones: effect of feed solids concentration. *Miner. Eng.* 31: 17-31.

27 Ghodrat, M.; Qi, Z.; Kuang, S. B., et al. (2016) Computational investigation of the effect of particle density on the multiphase flows and performance of hydrocyclone. *Miner. Eng.* 90:55-69.

28 Sripriya, R.; Kaulaskar, M. D.; Chakraborty, S., et al. (2007) Studies on the performance of a hydrocyclone and modeling for flow characterization in presence and absence of air core. *Chem. Eng. Sci.* 62:6391-6402.

29 Evans, W. K.; Suksangpanomrung, A.; Nowakowski, A. F.. (2008) The simulation of the flow within a hydrocyclone operating with an air core and with an inserted metal rod. *Chem. Eng. J.* 143:51-61.

30 Zou, J. ; Wang, C.; Ji, C.. (2016) Experimental study on the air core in a hydrocyclone. *Dry. Technol.* 34:854-860.

31 Marins, L. P. M.; Duarte, D. G.; Loureiro, J. B. R., et al. (2010) LDA and PIV characterization of the flow in a hydrocyclone without an air-core. *J. Petrol. Sci. Eng.* 70:168-176.

32 Cui, B.; Wei, D.; Gao, S., et al. (2014) Numerical and experimental studies of flow field in hydrocyclone with air core. *T. Nonferr. Metal. Soc.* 24:2642-2649.

33 Wen, C.Y.; Yu, Y.H.. (1966) Mechanics of fluidisation. *Chem. Eng. Prog. Symp. Ser.* 62:100-111.

34 Ergun, S.. (1952) Fluid flow through packed columns. *Chem. Eng. Prog.*48 (2):89-94

35 Xu, Y.; Song, X.; Sun, Z.,et al. (2013) Numerical investigation of the effect of the ratio of the vortex-finder diameter to the spigot diameter on the steady state of the air core in a hydrocyclone. *Ind. Eng. Chem. Res.* 52:5470-5478.

Figure captions:

Fig. 1 Geometrical structure of hydrocyclone with different feed body

Fig. 2 Mesh of hydrocyclone with different feed body

Fig. 3 Schematic of PIV test apparatus: (a) test rig (1-hydrocyclone with conical feed body; 2-transparent box; 3-water tank; 4-pump; 5-flowmeter; 6-pressure gauge) ; (b) PIV measurement system; (c) photo of hydrocyclone

Fig.4 Air-core formation

Fig.5 Velocity distribution at the bottom of vortex finder

Fig.6 Pressure distribution at different section

Fig. 7 Tangential velocity distribution at different section

Fig. 8 Axial velocity distribution at different section

Fig. 9 LZVV diagram

Fig. 10 Grade efficiency curve

Fig.11 Effect of Cone angle on flow field and separation performance in conical feed body

Fig.12 Effect of Cone angle on flow field and separation performance in tapered feed body

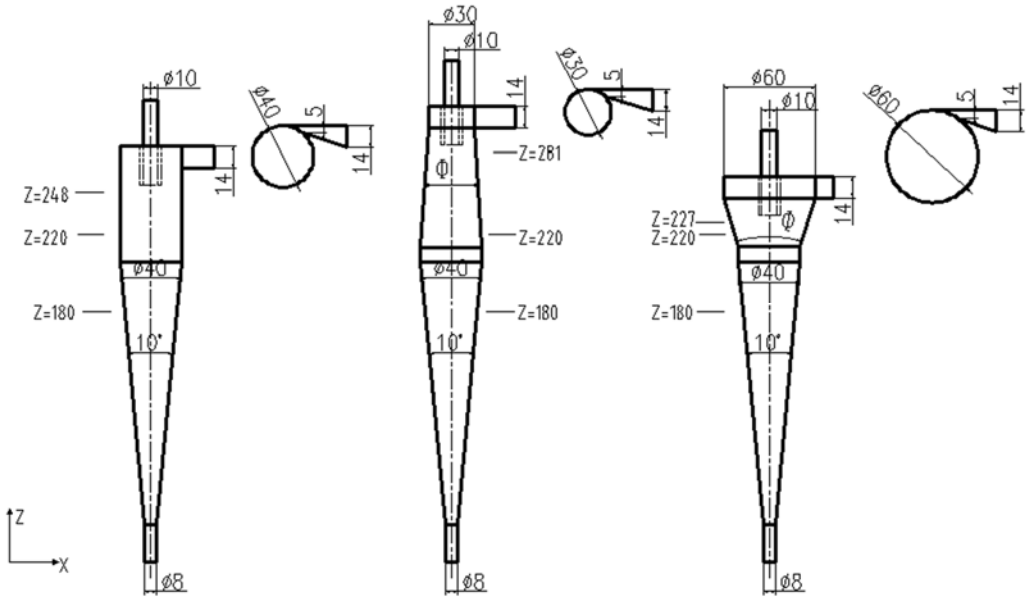

(a) cylindrical (b) conical (c) tapered

Fig. 1 Geometrical structure of hydrocyclone with different feed body

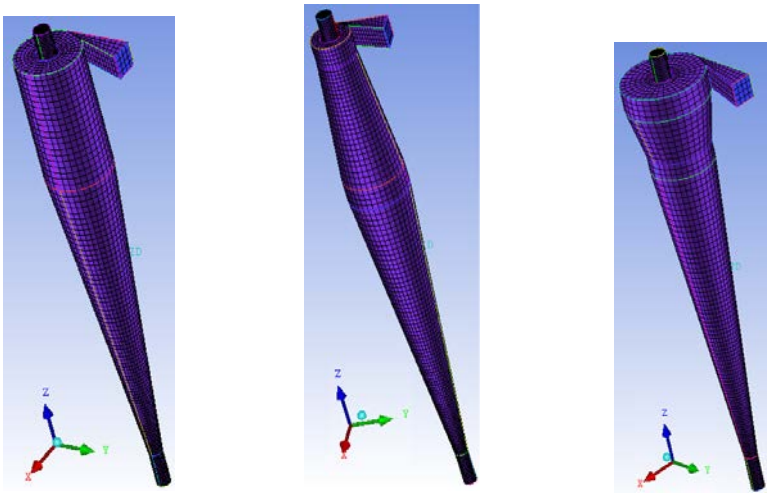

(a) cylindrical (b) conical (c) tapered

Fig. 2 Mesh of hydrocyclone with different feed body

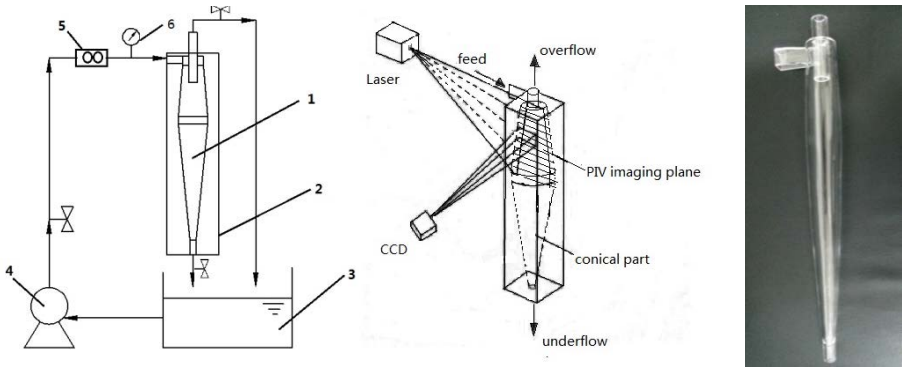

(a) (b) (c)

Fig. 3 Schematic of PIV test apparatus: (a) test rig (1-hydrocyclone with conical feed body; 2-transparent box; 3-water tank; 4-pump; 5-flowmeter; 6-pressure gauge) ; (b) PIV measurement system; (c) photo of hydrocyclone

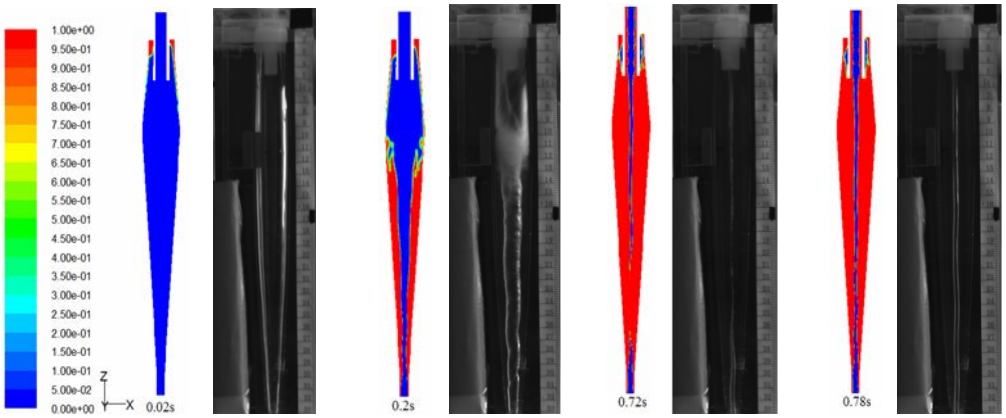

Fig.4 Air-core formation

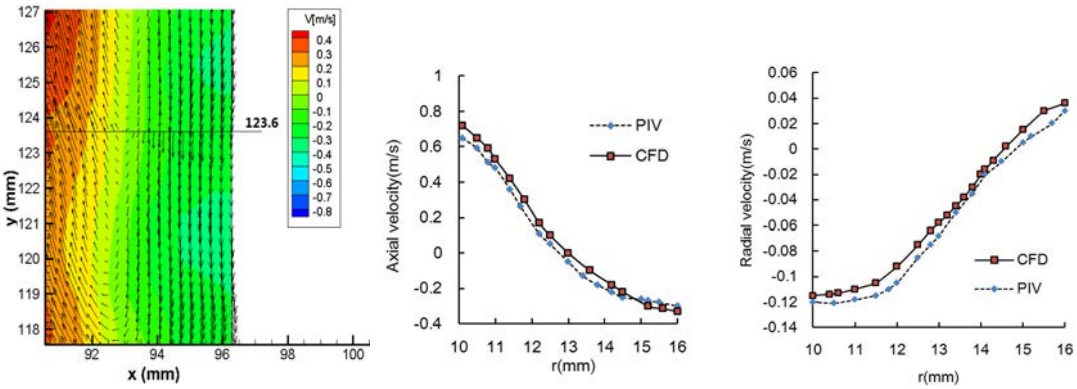

(a) velocity vector (b) axial velocity (c) radial velocity

Fig.5 Velocity distribution at the bottom of vortex finder

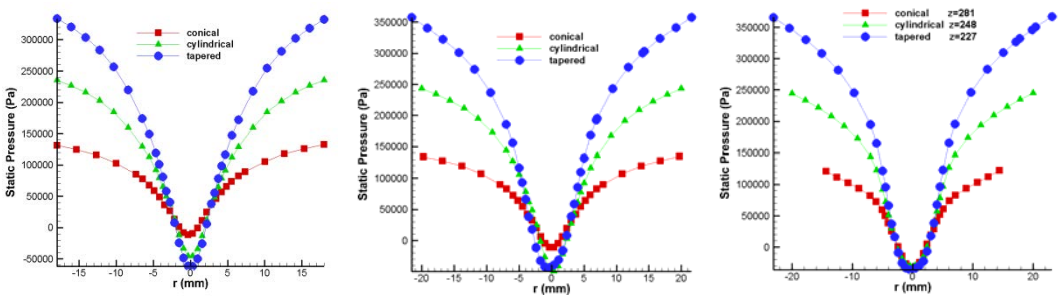

(a)z=180mm (b) z=220mm (c)z=281mm/248mm/227mm

Fig.6 Pressure distribution at different section

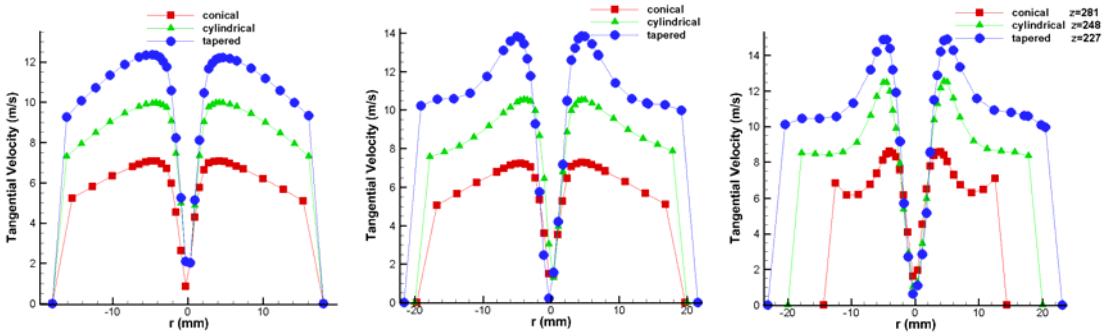

(a)z=180mm (b) z=220mm (c)z=281mm/248mm/227mm

Fig. 7 Tangential velocity distribution at different section

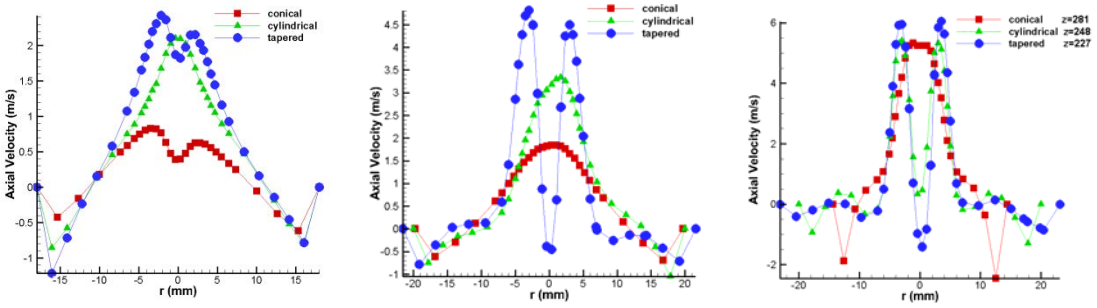

(a)z=180mm (b) z=220mm (c)z=281mm/248mm/227mm

Fig. 8 Axial velocity distribution at different section

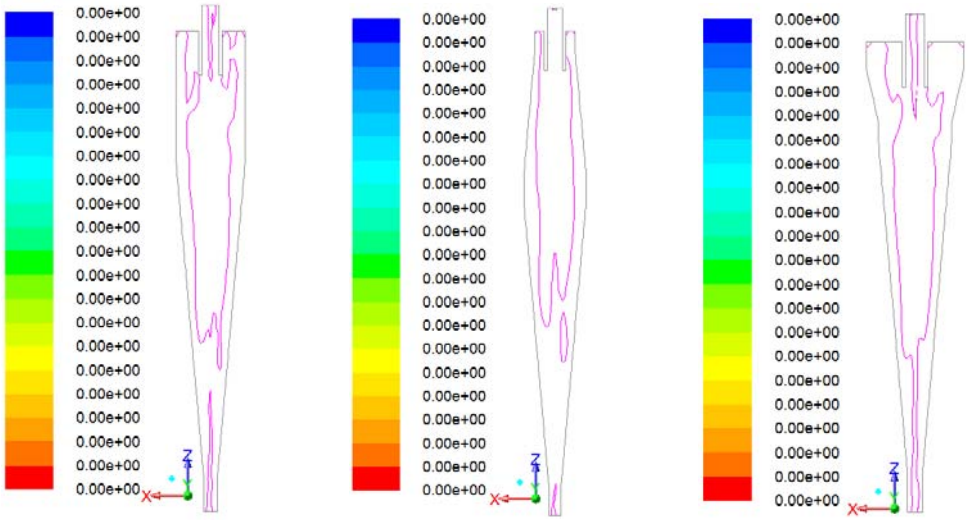

(a) cylindrical (b) conical (c) tapered

Fig. 9 LZVV diagram

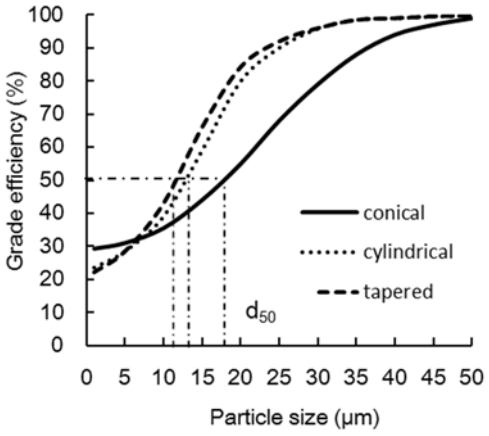

Fig. 10 Grade efficiency curve

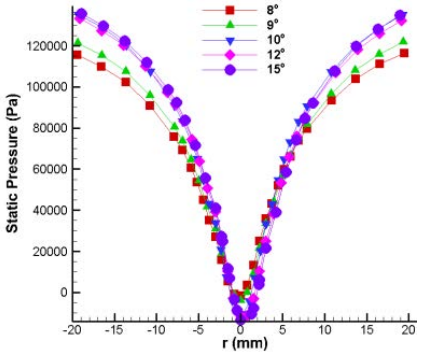

(a) static pressure

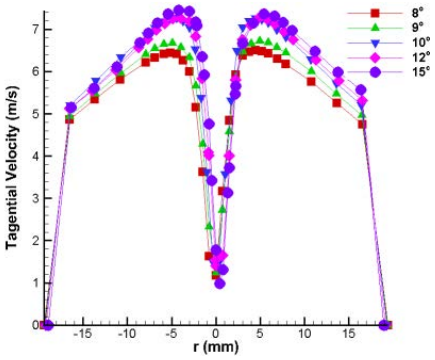

(b) tangential velocity

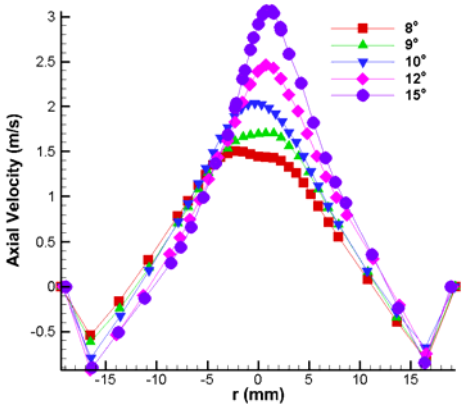

(c) axial velocity

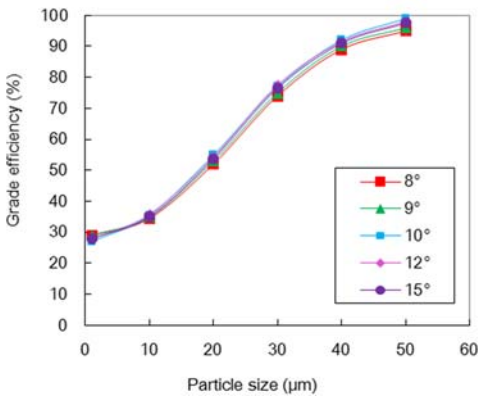

(d) grade efficiency

Fig.11 Effect of Cone angle on flow field and separation performance in conical feed body

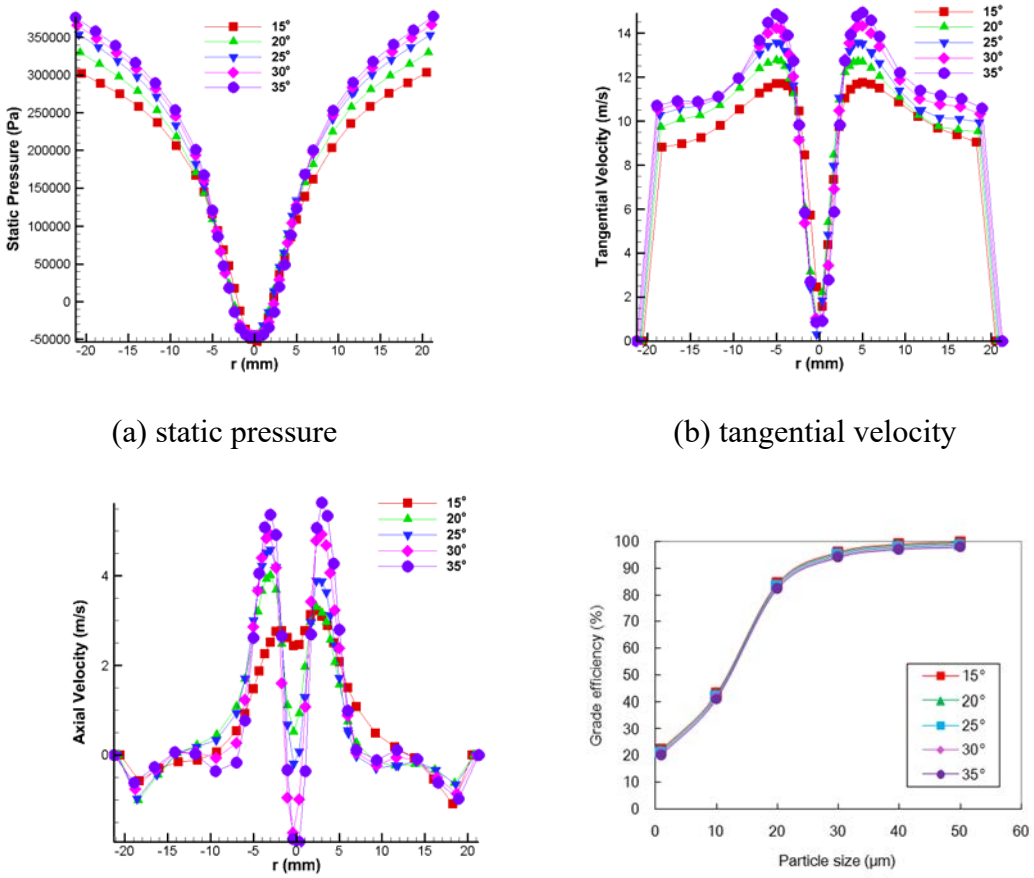

(a) static pressure

(b) tangential velocity

(c) axial velocity

(d) grade efficiency

Fig.12 Effect of Cone angle on flow field and separation performance in tapered feed body